

Cu and Ni functionalized hydroxyapatite biocomposites from common carp scales: green synthesis for antibacterial assessment and wastewater treatment

Amina Khalid*, Sana Zulfiqar, Maryam Abbasi

Department of Environmental Sciences, Fatima Jinnah Women University, Rawalpindi, Pakistan,
emails: aminakhalid004@gmail.com (A. Khalid), sanazulfiqar@fjwu.edu.pk (S. Zulfiqar), maryam.abbasi009@gmail.com (M. Abbasi)

Received 25 August 2020; Accepted 15 January 2021

ABSTRACT

Industrialization, urbanization and subsequent technological advancements in Pakistan has raised the pollution to threshold level. The current research was conducted with the aim to become the part of the solution not the part of pollution. Keeping in view the same objective, refused fish scales of common carp were used to extract hydroxyapatite (HAp) and then functionalized with metals (Cu and Ni) to synthesize the biocomposites. Samples were characterized using Fourier transform infrared spectroscopy, X-ray diffraction and X-ray fluorescence techniques, which confirmed the synthesis of the HAp, Cu-HAp (3 wt.%) and Ni-HAp (3 wt.%) biocomposites with the particle size of 17, 24 and 25 nm, respectively. The synthesized biocomposites were further employed as adsorbents for the removal of Malachite green (MG) and cadmium ions (Cd^{2+}) from the wastewater. Results showed that Ni-HAp 1:3 (1% metal) and Cu-HAp 1:3 (1% metal) acted as best adsorbents for the removal of MG and Cd^{2+} with the removal efficiency of 94%, respectively. Furthermore, the antibacterial nature of these biocomposites was also evaluated against the gram-positive bacterial strain (*Staphylococcus aureus*). Findings showed that selected biocomposites (Cu-HAp 1:1 (1 wt.% metal), Cu-HAp 3:1 (3 wt.% metal), Cu-HAp 1:3 (1 wt.% metal), Ni-HAp 1:1 (1 wt.% metal), Ni-HAp 3:1 (3 wt.% metal), Ni-HAp 1:3 (1 wt.% metal)) can act as the good antibacterial agents but Ni-HAp 3:1 (3 wt.% metal) was proven as best antibacterial agent with inhibition zone equal to 31 mm. Among adsorption isotherms and kinetics, Langmuir isotherm and pseudo-second order shows the best fitting for MG azo dye removal from wastewater whereas Freundlich isotherm and pseudo-first order is best fit for Cd^{2+} adsorption on both composites. Boyd plot shows the best fit for both the adsorbents.

Keywords: Hydroxyapatite; Biocomposites; Wastewater treatment; *Staphylococcus aureus*; Common Carp scales; Adsorption

1. Introduction

Human society faces vast challenges to access food and livings to the population of about 7.7 billion around the globe, while addressing the excessive impacts of environmental deterioration and climate change [1]. Safe drinking water and food availability are the basic necessities of life. With the increase in industrialization and advancement in technology, food production has increased but the quality of food has been compromised [2]. Due to this, a lot of contaminants enter the environment leading to more

waste generation, which subsequently results in health problems specifically in underdeveloped countries such as Pakistan [3].

The contaminants generated from many industries such as heavy metals [4] and azo dyes [5] are discharged in the water bodies ultimately result in the contamination of water resources posing serious threats to human health [6–8]. Due to increase in the water organic content, the growth of several pathogenic microflora, that is, *Salmonella* species, *E. coli*, *Staphylococcus aureus* species etc. also gets increased, resulting in major water-borne diseases [9–11]. According to

* Corresponding author.

the findings of Daud et al. [12], only 20% of the total population of Pakistan has access to safe drinking water and 50% of the diseases are caused by unclean drinking water followed by the average death rate of around 40% in the country. Waste generation from food industry also pollutes water and, in this regard, waste produced from fisheries and aquaculture industry is targeted. With increase in the demand for food, an exponential increase in aquaculture industry is also observed in the past years. According to the latest report from FAO of UN, global fisheries production in 2016 has reached 171 million tons [13] and Asia is responsible for 89% of the aquaculture waste in 2010, ultimately leading to environmental pollution.

The main waste from fisheries constitutes fish scales, which are made up of proteins, collagen and connective tissues covered with the salts of calcium [14,15]. These scales are naturally considered as an important source of calcium phosphate [Hydroxyapatite (HAp); $(\text{Ca}_{10}(\text{PO}_4)_6(\text{OH})_2)$], which is the natural bone and teeth material [16,17]. HAp is non-toxic, anti-inflammatory, non-immunogenic, bio-active and biocompatible and undertakes the process of osteointegration, which plays important role in bone tissue engineering [18–21].

HAp can be functionalized with metals such as zinc, silver, cobalt, iron, etc. to overcome the bacterial infections during implants, and to enhance its properties as potential adsorbents for various pollutants [22,23] especially for the remediation of water and several researches also reported the functionalized HAp with metals and polymers to enhance the rate of adsorption. Ma et al. [24] in 2009 reported the fabrication of Ag–TiO₂/hydroxyapatite/Al₂O₃ bioceramic composite membrane that aids in the effective adsorption of bacteria (*E. coli*) and its photocatalytic inactivation, which ultimately suggests its ability to treat bacterial contaminated groundwater and drinking water. Li et al. [25] also synthesized novel Ag₃PO₄-loaded hydroxyapatite (HAp) composites and reported that these materials are very effective in the adsorption of lead ions from wastewater and readily degrade the azo dyes (rhodamine B, methyl orange and methylene blue). Moreover, these composites also act as good antibacterial agents in case of *E. coli* and *S. aureus* [25]. Another composite adsorbent hydroxyapatite/magnetite (HAp/Fe₃O₄) has been synthesized by Dong et al. [26] to remove lead ions from water. Post experimental studies revealed that this composite can remove lead ions with the reported efficiency of 99% [26]. These evidences proved the ability of HAp composites as good adsorbents thus playing an important role in the treatment of wastewater by the process of adsorption.

To the best of our knowledge, it is the first research report presenting the synthesis of HAp from common carp scales by alkaline heat treatment, and Cu and Ni functionalized hydroxyapatite biocomposites via calcination method. Because of the good catalytic and antibacterial properties of Cu and Ni, these metals are selected for the synthesis of desired product. These biocomposites can also be used in bone implants and Cu plays important role in the maintenance of bone health and takes part in the interaction of more than 300 enzymes [27]. In the present research, these biocomposites are used as adsorbents for the removal of cadmium and Malachite green from wastewater as well

as antibacterial agents against the gram-positive bacterial strain (*S. aureus*).

2. Materials and methods

The research methodology comprises of the extraction of hydroxyapatite (HAp), synthesis of Cu-HAp and Ni-HAp biocomposites, isolation of a bacterial strain (*Staphylococcus aureus*), and catalase test. Disk diffusion method for antibacterial activity is also used in order to evaluate the antibacterial nature of synthesized biocomposites.

2.1. Extraction of hydroxyapatite (HAp)

The present study was conducted using methodology from already reported literature [14,17,28–30] with some modifications. Refused scales of common carp (Gulfam) were collected from fish selling point located in Rawat, Islamabad, Pakistan followed by cleaning, washing and air drying at room temperature for 2 d [17,30] and these scales were then used to extract hydroxyapatite (HAp) via acid treatment [14,28] and alkaline heat treatment [29].

The clean fish scales were initially deproteinized by soaking into 0.1 M HCl (Lab Scan, 37% w/v) solution for an hour followed by subsequent washing. In order to get white precipitates, 5% w/v NaOH (Salt of Scharlau, 40 g/mol) solution were added at 70°C for 7 h followed by filtration, washing and oven drying at 60°C, respectively [29]. Further, hydroxyapatite was extracted from treated material using NaOH (Salt of Scharlau, 40 g/mol) solution (50% w/v) under 800 rpm at 80°C for an hour. The HAp obtained was filtered, washed several times with deionized water to reduce its alkaline nature and dried at 100°C [28]. The resultant coarse product was ground in order to obtain homogenized/refined hydroxyapatite powder, which was then coded as HAp (CC) [14,17].

2.2. Synthesis of Cu-HAp (CC) and Ni-HAp (CC) biocomposites

Extracted HAp powder was mixed with copper sulfate (Riedel-deHaen, CuSO₄·5H₂O-249.68 g/mol) and nickel sulfate (Riedel-deHaen, NiSO₄-262.85 g/mol) separately in varying proportions (1–3 wt.%) for preparation of the biocomposites (Cu-HAp and Ni-HAp). The homogeneous mixing of metal salts with hydroxyapatite was carried out by using mortar and pestle for almost 20 min and calcination was done in electric furnace at 800°C for 1 h to acquire the interacted Cu-HAp and Ni-HAp biocomposites. Furthermore, uniaxial press was used to make the pellets (disks) of these biocomposites and baked them in an electric oven at 200°C for almost 3 h, which were then used for antibacterial evaluation tests.

2.3. Isolation of *Staphylococcus aureus* (gram positive bacterial strain)

Staphylococcus aureus is a commonly known human pathogen and belongs to the genus of gram positive non-spore-forming cocci. In the current research, *S. aureus* was isolated from the milk samples. Mannitol salt agar (MSA, Bioworld, Dublin, USA, 111 g/L) was used as selective,

differential and indicator media for this purpose. MSA media was prepared, autoclaved and poured in separate petri plates by pour plate method. After this, the dilution factor of 10^6 was applied by using sterile saline solution and milk sample, followed by the spreading of these dilutions on agar plates in duplicates. The plates were then incubated at 37°C for 24–48 h.

Staphylococcus aureus has an ability to ferment mannitol sugar (the only source of carbohydrates) producing the pigments of deep yellow color on MSA plates [31]. After 24 h of incubation, the round yellow colonies of *S. aureus* had been identified on the agar plates based on morphological characteristics of the appeared colonies as shown in Fig. 1. The colonies were further streaked onto other plate containing MSA and incubated for 24–48 h to observe the lawns of the desired bacterial specie as shown in Fig. 2.

2.4. Catalase test

This test was conducted to confirm the isolated strains of *S. aureus*. Pure culture of *S. aureus* was swabbed on the glass slide with cotton swab and a droplet of hydrogen peroxide (Scharlau, 30% w/w, extra pure) was dropped on that culture. The appearance of bubbles instantly confirmed the presence of *S. aureus* (catalase producing bacteria), which broke down hydrogen peroxide into water and oxygen (Fig. S1). The reaction is as follows:

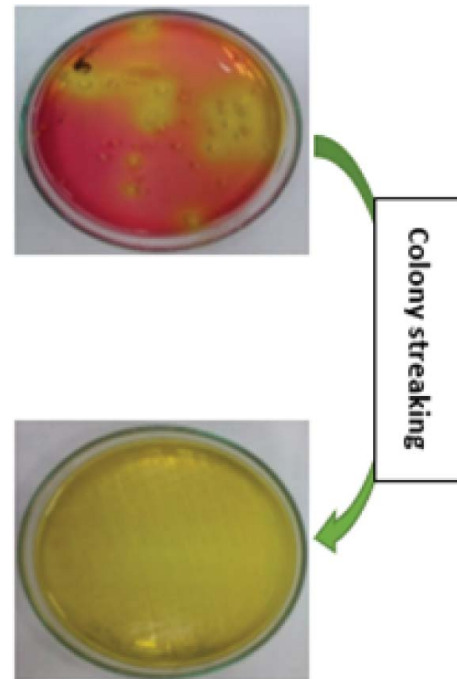


2.5. Antibacterial activity test (disk diffusion method)

The isolated strains of *S. aureus* (gram positive) were used to perform disk diffusion method. Colonies of the bacterial strain were picked with the help of sterile cotton swabs/inoculating loop and streaked on separate agar plates of Muller Hinton Agar (MHA, Merck, Germany, 34.0 g/L). The prepared disks of all the previously mentioned composites were placed on that agar plates carefully under complete sterilized conditions and incubated at 37°C , for 24–48 h, without inversion [17].

2.6. Batch adsorption experiments

The ability of prepared adsorbents to remove Cd^{2+} and azo dye (Malachite Green) from aqueous solutions was evaluated by batch adsorption experiments. In the current research, close batch experiments were conducted because of their environment friendly nature and among the different synthesized composites, only two were selected as adsorbents because of their good adsorption capacity. Three concentrations of Cd^{2+} (0.1, 0.3, 0.5 ppm) were taken whereas for malachite green (MG), concentrations of 0.01, 0.03 and 0.05 ppm were selected to carry out further experiments. Each experiment was conducted for 60 min with the time lapse of 5 min at optimal conditions. The dose of each adsorbent was kept as 20 mg and was added in working solutions. An aliquot of 5 mL was taken out from that solution after every 5 min, filtered by using syringe filters and then analyzed by flame atomic absorption spectrophotometer (FAAS) (Shimadzu, Japan, Model: A7000F) and



Figs. 1 & 2. Yellow colonies of *Staphylococcus aureus* on mannitol salt agar showing fermentation. *Staphylococcus aureus* lawn on mannitol salt agar plate.

UV-visible spectrophotometer (Shimadzu, Japan, Model: UV-1601). By using the following equation stock solutions and working solutions were prepared:

$$C_1V_1 = C_2V_2 \quad (2)$$

where C_1 is volume of stock solution, V_1 is required volume, which is to be calculated, C_2 is required solution and V_2 is required volume of solvent.

Percentage removal (removal efficiency) of pollutants and adsorption capacity was calculated by using the following equations, respectively:

$$\%R = \frac{C_i - C_f}{C_f} \times 100 \quad (3)$$

$$q_{\max} = \frac{C_i - C_f}{m} \times V \quad (4)$$

where C_i is initial concentration and C_f is final concentration of the solution, q_{\max} is adsorption capacity, V is volume of adsorbate and m is mass of adsorbent.

2.7. Adsorption isotherms and kinetic models

The process of understanding the nature of adsorption and surface properties through graphs is known as adsorption isotherms and kinetic models. These models are necessary for the clear and detailed understanding of the mechanism and rate of the uptake of pollutants on the

surface of adsorbents. In the current research, Langmuir isotherm, Freundlich isotherm, pseudo-second order kinetics, first order kinetics and Boyd plot were applied to assess the kinetic studies of the adsorption mechanism.

The linear form of Langmuir model is expressed in Eq. (5) as:

$$\frac{C_e}{q_e} = \frac{1}{Kq_{\max}} + \frac{1}{q_{\max}C_e} \quad (5)$$

where C_e is the equilibrium concentration of adsorbate, q_e is the amount of adsorbate adsorbed per unit mass of adsorbent, K is Langmuir constant (L/mg) and q_{\max} is maximum adsorption capacity (mg/g) [32,23]. The value of R^2 is 1 or close to 1 for the adsorption capacity of composites if the model fits well.

The following equation is used for the description of Freundlich isotherm.

$$\log q_e = \log K_f + \left(\frac{1}{n}\right) \log C_e \quad (6)$$

where C_e is the concentration of adsorbate at equilibrium, q_e is the amount of adsorbate adsorbed per unit mass of adsorbent, K_f is Freundlich constant and n is the constant, which shows intensity of adsorption [32].

The linear form of the pseudo-second order kinetic model is as in Eq. (7):

$$\frac{t}{q_i} = \frac{1}{K_2q_e^2} + \frac{1}{q_e}t \quad (7)$$

where K_2 represents the constant, q_e shows the adsorptive capability of adsorbent at equilibrium, q_i shows the concentration of adsorbent at time t [33].

Eq. (8) describes the pseudo-first order linear kinetic model:

$$\log(q_e - q_i) = \log q_e - \left(\frac{k_1}{2.303}\right)t \quad (8)$$

where q_e and q_i are the uptake amounts of adsorbates adsorbed (mg/g) at equilibrium and at time t (min) and k_1 is the pseudo-first order adsorption rate constant (min^{-1}) [34].

Boyd plot was also applied to check the adsorption pattern and slow step of the overall adsorption process. The linear form of it is given below:

$$B_t = -0.497 - \ln(1 - F) \quad (9)$$

where F is the fraction of solute sorbed at different times t [35].

2.8. Characterization

Samples were characterized by different techniques to confirm the synthesis of desired biocomposites. Fourier transform infrared spectroscopy (FTIR) (8400, Shimadzu, Japan) for the identification of functional groups present in

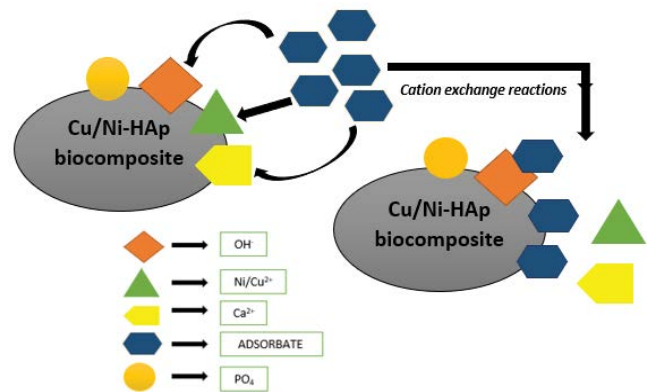


Fig. 3. Hypothetical model showing the adsorption mechanism of Cd^{2+} and MG by Cu/Ni-hydroxyapatite (HAp) biocomposites.

the sample while X-ray diffraction spectroscopy was used to determine the phase angle as well as particle size. Elemental composition of the desired samples was determined by X-ray fluorescence spectroscopy (Oxford Instruments X-MET 8000 Expert XRF Analyzer, UK). To evaluate the success of adsorption experiments, two different analytical techniques, UV-visible spectrophotometer (Shimadzu, Japan, Model: UV-1601) and FAAS (Shimadzu, Japan, Model: A7000F) were used to assess the removal efficiencies of MG and Cd^{2+} metal, respectively.

2.9. Hypothetical adsorption mechanism

Fig. 3 shows the hypothetical model for the mechanism of adsorption of Cd^{2+} and malachite green by Cu and Ni-HAp biocomposites.

3. Results and discussion

3.1. Fourier transform infrared spectroscopy

In the current research, FTIR technique was used to detect the functional groups present in the HAp and metal-HAp biocomposites synthesized from the common carp scales. Fig. 5a illustrates the FTIR spectrum of HAp (CC). The broad peak at $3,416.05 \text{ cm}^{-1}$ demonstrates the stretching vibrations of hydroxyl group (O–H) supported by researchers in the literature [36]. The peak, which appeared at $1,662$ and $1,465 \text{ cm}^{-1}$, corresponds to the trapped molecules of water (H_2O) and carbonates group (CO_3^{2-}), respectively. The indicated carbonated group confirms the type B carbonate group because the carbonate ions can be a good substitution for phosphate ions as reported by the literature [29]. The bands observed at $1,043$ and 565 cm^{-1} represents the presence of phosphate group (O–P–O) stretching vibrations [37]. The peak at 603 cm^{-1} represents the bending vibrations of phosphate group.

Figs. 5b and c show the overlay spectra of Cu-HAp (1–3 wt.%) and Ni-HAp biocomposites, respectively. The broad bands of water appeared at $2,500\text{--}3,416 \text{ cm}^{-1}$ in the spectrum of raw HAp gets decreased in Cu/Ni-HAp biocomposites due to calcination treatment. Results show that as the wt.% of Cu and Ni metal in HAp increases, the

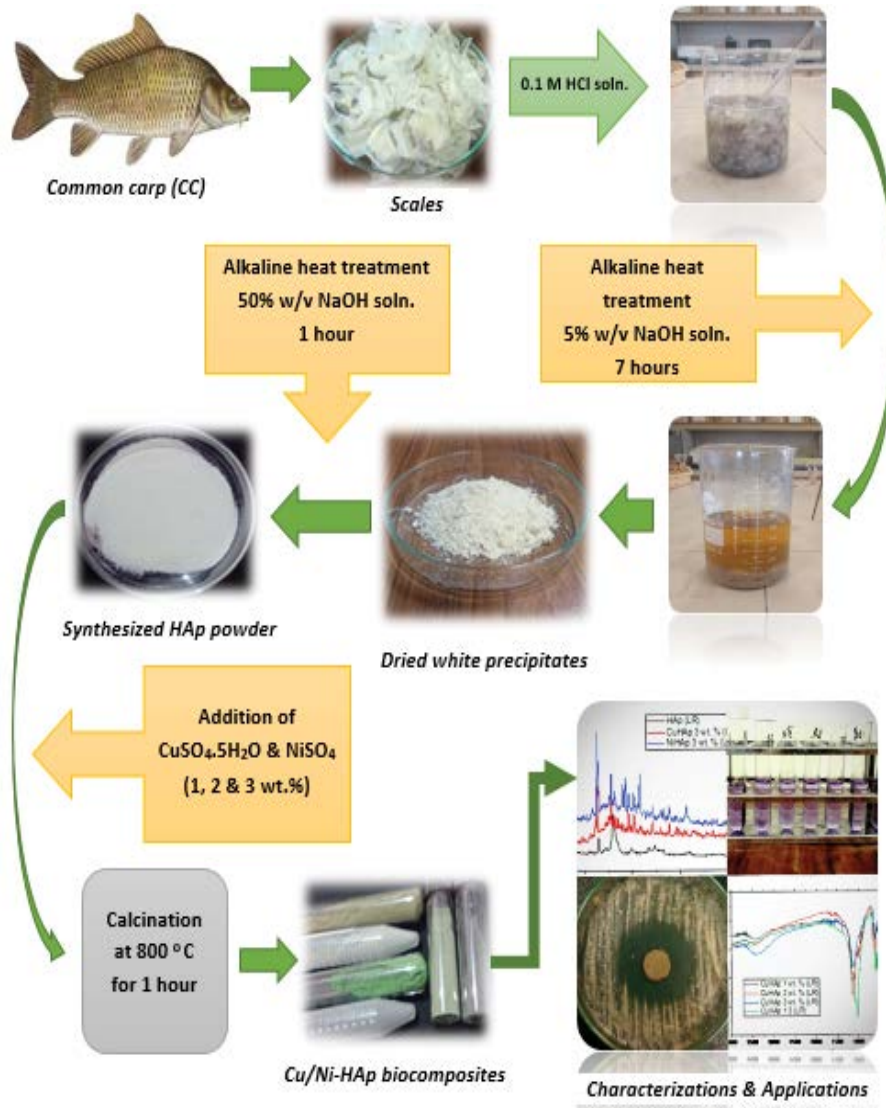


Fig. 4. Schematic representation of our work.

bands get decreased accordingly. Same results were also reported by Sathiskumar et al. [17]. The incorporation of copper and nickel metals in the structure of HAP results in low crystallinity (to view all the functional groups present in HAP, Table S1).

3.2. X-ray diffraction

Crystalline and amorphous nature of the raw material and composites were determined by the XRD analysis. Fig. 5d shows the XRD spectra of HAP and metal HAP biocomposites. The high intensity peaks represent the crystalline nature and the broad peaks/low intensity peaks indicate the amorphous nature of the sample. According to literature, HAP exhibits hexagonal crystalline structure system [38–41]. The spectrum of HAP shows the characteristic peaks of the sample while in the spectra of Cu-HAP and Ni-HAP biocomposites, these peaks get broader because of the incorporation of metals. In the spectrum of Cu-HAP

biocomposite, some new peaks, at 2θ range of 38° – 45° , were observed for metallic copper. These findings are consistent with the results of Yurieva et al. [42]. The new peaks observed at 2θ range of 35° – 45° and 61° show the Bragg's reflections due to nickel metal as reported by literature [43,44]. The crystallite size of the characterized samples was calculated by Debye–Scherrer equation. Eq. (10) is as follows:

$$D = \frac{k\lambda}{\beta \cos\theta} \quad (10)$$

where D shows crystallite size in nm, K is constant, λ is the wavelength of X-ray, β is the full width half maximum in radians and theta shows the peak position [45]. The average crystallite size of HAP, Cu-HAP (3 wt.%) and Ni-HAP (3 wt.%) biocomposites is 17, 24 and 25 nm, respectively, according to the analyzed results (Table S2).

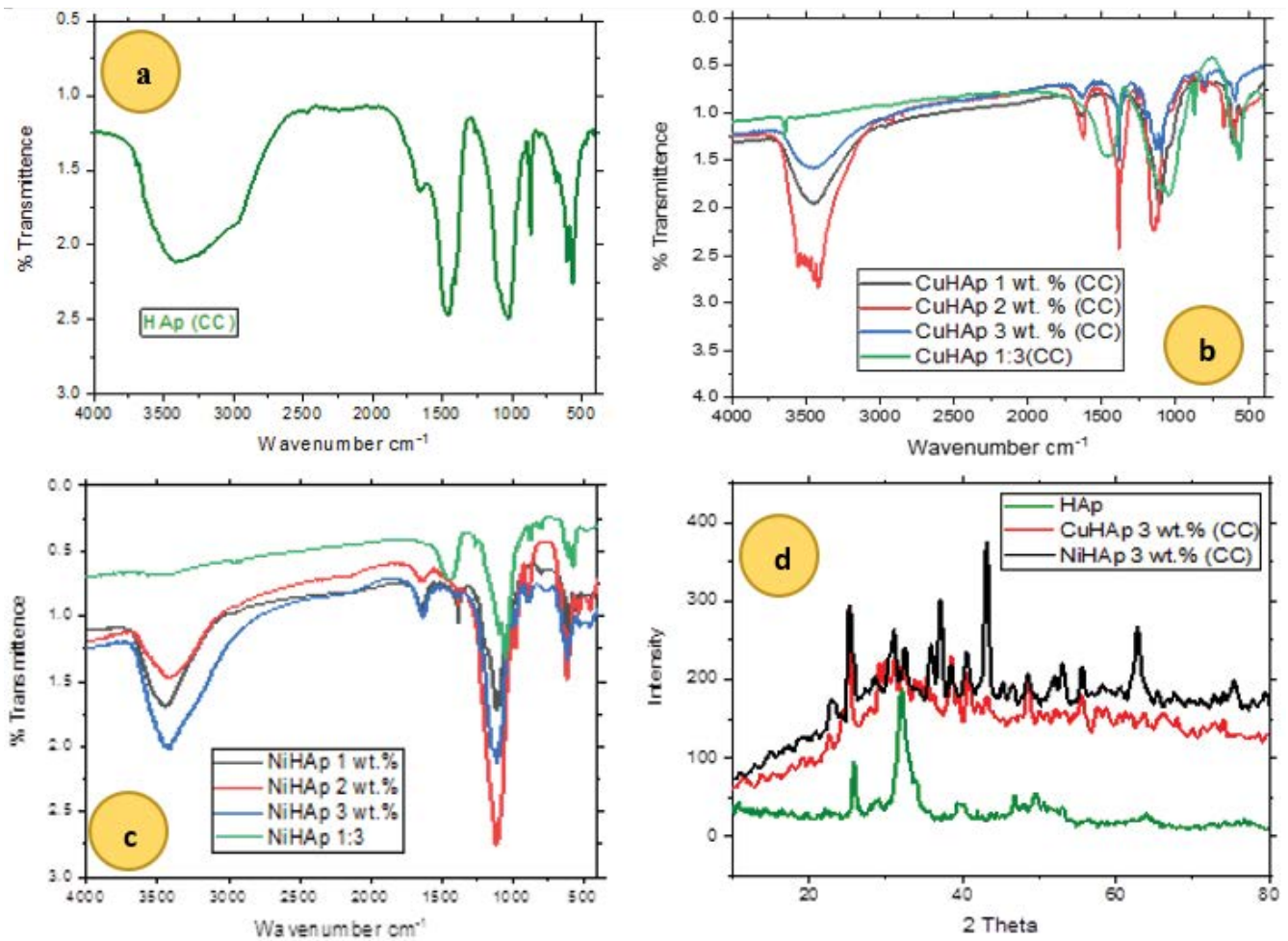


Fig. 5. (a) FTIR spectrum of HAp (CC), (b) overlay spectra of CuHAp (CC) biocomposites, (c) overlay spectra of NiHAp (CC) biocomposites, and (d) X-ray diffraction overlay spectra of HAp (CC) biocomposites.

3.3. X-ray fluorescence (XRF) analysis

In the current research, HAp and metal HAp biocomposites (at all weight percentages) were characterized by XRF analyzer, at the calibrations of plastic FP and alloy LEFP, to investigate the percentage of metals and basic elements present in the raw samples as well as in biocomposites. According to the recorded data, the most abundant elements present in the raw HAp samples are calcium and phosphorous and, in the metal-HAp biocomposites, quantity of desired metals is also present indicating the metal functionalization and formation of desired product. Several trace metals were also found in minute quantities.

Table 1 shows the elemental composition detected by XRF gun analyzer for all the samples.

3.4. Adsorptive removal of cadmium ions (Cd^{2+})

Cadmium (Cd^{2+}) is a heavy metal and gets released in environment by many natural and anthropogenic sources as industrial waste from smelting process, dye and electrochemical industries [46]. It is harmful for living entities and it specifically targets the bones and most susceptible

organs, that is, kidneys and liver, of living organisms [47]. The Cu-HAp (CC) 1:3 and Ni-HAp (CC) 1:3 biocomposites proved to be good adsorbents to remove Cd^{2+} from wastewater. Hydroxyapatite has many welcoming binding sites (mainly OH^-) [40] that undergo substitutions and make it efficient as adsorbent. Cation exchange reactions occur and Cd^{2+} ions get substituted with Ca^{2+} ions as shown in Fig. 3.

3.4.1. Effect of adsorbent with respect to time

One of the important parameters to study the adsorptive removal of biocomposites is the function of time (min) [48]. Porosity and number of available active binding sites, on the surface of adsorbents, play vital role in adsorption. Results showed an increase in adsorption efficiency with increase in time [49] from 0 to 40 min until first dynamic equilibrium was achieved. After this time, an increase–decrease sorption process was noted, which can be attributed towards rapid adsorption–desorption phenomenon and attainment of dynamic equilibrium. Maximum adsorption efficiency of 94% was observed at 0.1 ppm in case of Cu-HAp 1:3 (CC).

Table 1
Percentage of elements present in raw HAp and Cu/Ni-HAp biocomposites

Samples	Percentage of elements							
	Ca	Sr	Sn	P	Fe	Zn	Ni	Cu
HAp (CC)	7.75	0.98	0.02	69.24	1.42	0.59	–	–
CuHAp 1 wt.% (CC)	6.63	0.73	0.02	7.93	0.02	0.02	0.01	12
CuHAp 3 wt.% (CC)	4.89	0.67	0.02	0.25	0.02	0.04	0.04	25.3
CuHAp 1:3 (CC)	8.17	–	0.38	12.45	–	0.08	–	13
NiHAp 1 wt.% (CC)	6.57	0.98	0.01	8.71	–	0.02	51	–
NiHAp 3 wt.% (CC)	3.33	0.54	0.02	0.55	0.02	0.01	45	–
NiHAp 1:3 (CC)	5.87	–	–	8.84	–	0.19	28.30	–

3.4.2. Effect of concentration

Relative concentration of adsorbate is another crucial parameter to evaluate the adsorption efficiency of adsorbents. Effect of concentration of Cd^{2+} on the adsorptive nature of biocomposites was observed at 0.1, 0.3, 0.5 ppm by keeping the dosage (20 mg) of adsorbent constant throughout the experiment. It has been observed that with an increase in dye concentration, the % removal gets decreased indicating an inverse relation between adsorbate and adsorbent. Decrease in adsorption shows that all the binding sites were already occupied, and no space was left on the surface of adsorbent for further adsorption [50].

According to findings, the Cu/Ni-HAp (CC) biocomposites show the best removal efficiency towards the removal of Cd^{2+} because of high porosity and active binding sites, by cation exchange reactions. CuHAP 1:3 (CC) has the best removal efficiency towards cadmium as compared with other composites because of its active binding sites available on the surface. The overall trend towards cadmium removal by the synthesized adsorbents is as under:

$$\text{Cu-HAp 1:3 (CC) } 94\% > \text{Ni-HAp (CC) } 91\% \quad (11)$$

Figs. 6a and b show the removal of cadmium by the synthesized adsorbents, respectively.

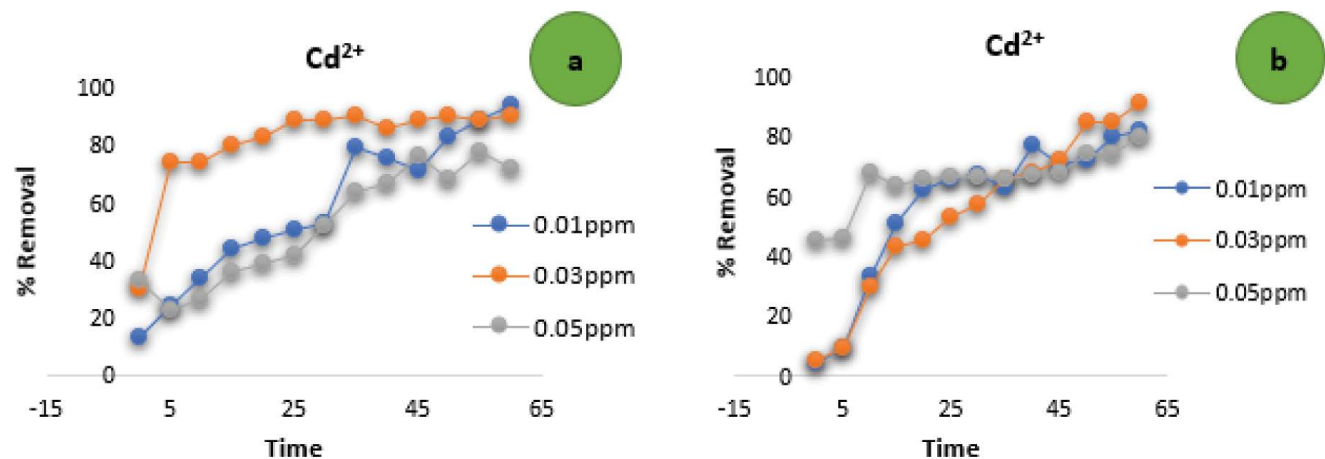


Fig. 6. (a) Graph of Cd^{2+} with CuHAp 1:3 (CC) and (b) Graph of Cd^{2+} with NiHAp 1:3 (CC).

3.5. Adsorptive removal of azo dyes

Malachite green is a cationic dye, basic in nature and has positive charge on it. The positive charge shows that it has the property to either gain hydrogen or lose hydroxide ion in water. Carcinogenic effects in the immune system and reproductive system of those fishes have been reported, which has been treated with malachite green dye [51]. Structure of malachite green contains many functional groups, which ultimately made it possible for the adsorption on the surface of synthesized adsorbents [50].

HAp consists of tetrahedral phosphate group, where four oxygen atoms surround one phosphate atom and this tetrahedron is surrounded by calcium ions. The sites containing calcium ions are of special interest because they act as host of hydroxyl ions (OH^-). The area, which covers the OH^- sites, is very much susceptible for substitutions by controlling the acid–base sites. HAp, with the molar ratio of 1.57, behaves similar to an acid catalyst having the existing basic sites [40]. The existence of these evacuated sites in the structure of hydroxyapatite possibly plays the role in adsorption of pollutants such as azo dyes.

3.5.1. Effect of time

The effect of time was studied and the percentage removal of MG dye was calculated, keeping the dosage

of adsorbent as 20 mg at the concentration of 0.01, 0.03, 0.05 ppm solution. All the other parameters (dose of adsorbent, pH, temperature) were kept constant except the contact time. The rate of adsorption got decreased with increase in time and removal efficiency got increased as the time increased [52] and at some point, equilibrium was achieved which gives the information about the possible saturation of sites after which adsorption and desorption both can occur simultaneously as shown in Figs. 7a and b.

3.5.2. Effect of concentration

The concentration of MG solution is considered as an important parameter, which may impact the adsorption efficiency of the adsorbents [53]. Adsorption efficiency was calculated on three different concentrations of MG (0.01, 0.03, 0.05 ppm) at the constant dose of 20 mg for each adsorbent. It is evident from the results that increase in dye concentration leads to decrease in removal efficiency of the adsorbents. Similar results in the process of adsorption were reported by other researchers [54]. The removal efficiency is high in 0.01 ppm concentration of adsorbate. Taking one aliquot from the solution at different times, the solution volume will be changed but it does not affect the residual concentration of pollutants in the solution because the desired aliquot was taken from the optimized concentration, prepared from stock solution of 1,000 ppm.

Both biocomposites showed good removal efficiency towards the cationic dyes (Malachite Green). NiHAp 1:3 (CC) acted as the best composite for the removal of MG with the removal efficiency of 94% followed by CuHAP 1:3 (CC). The overall trend is as under:

$$\text{NiHAp 1:3 (CC) } 94\% > \text{CuHAP 1:3 (CC) } 83\% \quad (12)$$

Figs. 7a and b show the removal of Malachite green by the synthesized adsorbents, respectively.

3.6. Antibacterial activity of synthesized biocomposites

Antibacterial activity of the synthesized biocomposites had been studied by disk diffusion method and the results

conclude that, after 24 h of incubation, the plates were taken out from the incubator and bacterial inhibition zones were observed and measured in mm. The inhibition zone got increased with the increase in the weight percentage of metals in biocomposites, which ultimately point out the antibacterial nature of the synthesized biocomposites as proposed in the literature. Several mechanisms were assumed by scientists, which show the process of the reduction of bacterial growth by initiating cell death and carry out several structural changes in the membrane proteins of bacteria as reported by the literature [55].

Table 2 illustrates the inhibition zones of all biocomposites with *S. aureus*, highly pathogenic gram-positive bacterial strain and Ni-HAp 3:1 (3 wt.% metal) was proved as best antibacterial agent with inhibition zone equal to 31 mm (For inhibition zones, see Fig. S2).

3.7. Kinetic models and adsorption isotherms

The adsorption isotherms are used to predict the adsorption patterns of the process and kinetic modeling is used to predict and explain the rate of adsorption and adsorption mechanisms. Langmuir isotherm indicates the monolayer adsorption patterns while Freundlich isotherm suggests the multilayer adsorption patterns as reported in literature [57]. In the regard of kinetics, the pseudo-first order kinetic model explains the relationship between the rate the sorption sites of the adsorbents are occupied and the number of unoccupied sites. This model is characteristic for physical adsorption while the pseudo-second order kinetic model can be used to describe one chemical adsorption process [58]. According to the results, it was observed that the synthesized biocomposites exhibit monolayer and multilayer adsorption, which generally shows that the sites required for the adsorption are equal and pollutants are immovable at the surface of adsorbents as well as surface of the adsorbent is heterogenous in nature [53]. For the adsorption of Cd^{2+} , the phenomena of multilayer adsorption were observed for both composites. Whereas in case of Malachite Green adsorption, all composites exhibit monolayer and multilayer adsorption except NiHAp 1:3 (CC), which shows only monolayer adsorption pattern because of the saturation

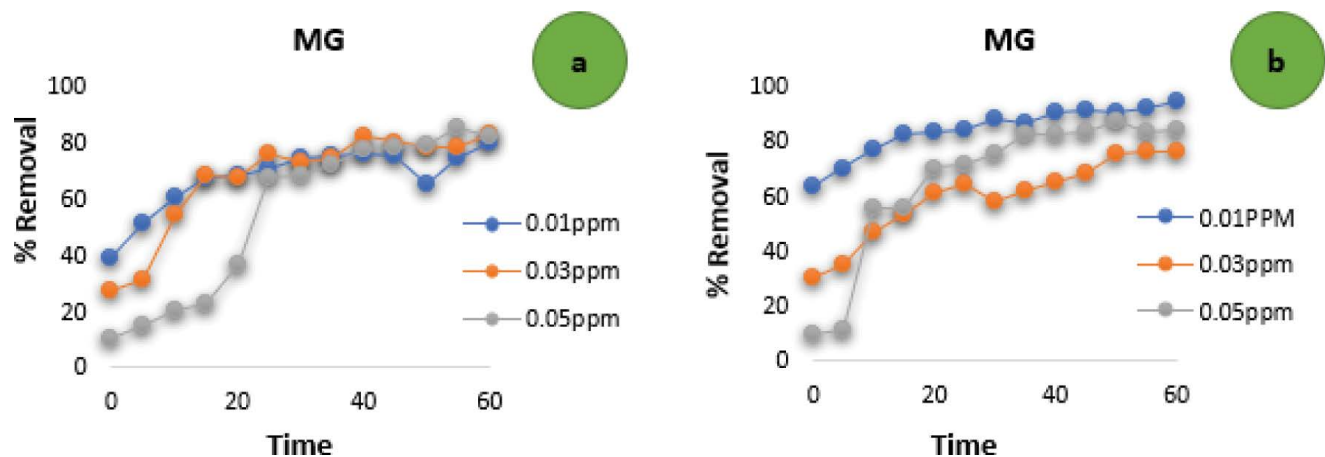


Fig. 7. (a) MG with CuHAP 1:3 (CC) and (b) MG with NiHAp 1:3 (CC).

of all adsorption sites at the surface and non-availability of more binding sites. Results demonstrated that the synthesized composites followed the pseudo-second order reaction for malachite green adsorption and pseudo-first order for Cd²⁺ adsorption on both composites. Boyd plot also showed good regression values in case of malachite green adsorption and Cd²⁺ adsorption by both composites, respectively. CuHAp 1:3 (CC) showed best value of 0.9472 in case of Cd²⁺ adsorption.

Table 3 shows the summarized results of adsorption isotherms and kinetic models (see Figs. S3–S7, which show the graphical representations of Langmuir and Freundlich isotherms, pseudo-second order and pseudo-first order kinetics and Boyd plot, respectively).

4. Conclusion

Hydroxyapatite (HAp) and Cu/Ni-HAp biocomposites were synthesized successfully from common carp scales in a cost effective and ecofriendly manner. It is concluded from the analysis that all the synthesized biocomposites showed best removal efficiency towards the cadmium, malachite green dye and brought a novel and unique approach towards the wastewater treatment and in biomedical field as well.

- FTIR bands, XRD spectra and XRF analysis confirmed the formation of the desired products.
- CuHAp 1:3 (CC) showed highest removal efficiency (94%) towards Cd²⁺ as compared with other biocomposites.
- NiHAp 1:3 (CC) acted as the best composite as compared with other synthesized biocomposites, with the removal

efficiency of 94% at the concentration of 0.01 ppm for the adsorptive removal of malachite green.

- All the biocomposites showed best trends toward the monolayer and multilayer adsorption while biocomposites of metal-HAp (CC) showed the best fit in case of pseudo-second order reaction for the removal of dyes.
- The synthesized biocomposites showed excellent antibacterial properties. In case of bacterial growth inhibition, among all biocomposites, Ni-HAp 3:1 (3 wt.% metal) acted as the best biocomposites with the inhibition zone of 31 mm for *S. aureus* species.

5. Recommendations

HAp is the vital constituent of living bodies and plenty of its uses and applications are explored by the researchers but there is still room for further research on its compounds. Scientists can explore this compound further by doping and functionalizing with other compounds to make it more efficient and suitable adsorbent for many contaminants such as dioxins, polychlorinated biphenyl, colored water (dyes contaminated water), many heavy metals and pesticides from different environmental compartments. Metal HAp biocomposites possess antibacterial properties but their antimicrobial properties can also be explored that will aid in killing several hazardous species of microbes thus revolutionizing the biomedical field. Regeneration and desorption studies of synthesized materials will also be carried out after applications. Commercial level applications of these adsorbents are encouraged and biosynthesis of these biocomposites will be helpful in promoting green environment.

Table 2
Inhibition zones (mm) of biocomposites (CC) with *Staphylococcus aureus*

S. no.	Metal HAp biocomposites (CC)	Inhibition zones (mm) of biocomposites (CC) with <i>Staphylococcus aureus</i>
01.	Cu-HAp 1:1 (1 wt.% metal)	20
02.	Cu-HAp 3:1 (3 wt.% metal)	28
03.	Cu-HAp 1:3 (1 wt.% metal)	25
04.	Ni-HAp 1:1 (1 wt.% metal)	22
05.	Ni-HAp 3:1 (3 wt.% metal)	31
06.	Ni-HAp 1:3 (1 wt.% metal)	21

Table 3
Summarized results of adsorption isotherms and kinetic models

Isotherms and kinetic models	Parameters	Malachite green		Cadmium ions (Cd ²⁺)	
		Cu-HAp 1:3(CC)	Ni-HAp 1:3(CC)	Cu-HAp 1:3(CC)	Ni-HAp 1:3(CC)
Langmuir isotherm	R ²	0.95	0.74	0.62	0.80
	q _{max}	6.11	-10.66	3.08	5.11
Freundlich isotherm	R ²	0.99	0.24	0.70	0.97
Pseudo-first order	R ²	0.72	0.87	0.93	0.92
Pseudo-second order	R ²	0.98	0.99	0.83	0.65
Boyd model	R ²	0.77	0.80	0.94	0.72

Acknowledgments

Special thanks to Fatima Jinnah Women University, Rawalpindi, Pakistan and Pakistan Environmental Protection Agency, Islamabad (Pak-EPA) for the cooperation and facilitation of research labs and support during the whole research period.

References

- [1] M. Balasubramanian, Climate change, famine, and low-income communities challenge Sustainable Development Goals, *Lancet Planet. Health*, 2 (2018) e421–e422.
- [2] N. Ramankutty, Z. Mehrabi, K. Waha, L. Jarvis, C. Kremen, M. Herrero, L.H. Rieseberg, Trends in global agricultural land use: implications for environmental health and food security, *Annu. Rev. Plant Biol.*, 69 (2018) 789–815.
- [3] S.A. Khan, M. Suleman, M. Asad, Assessment of pollution load in marble wastewater in Khairabad, District Nowshera, Khyber Pukhtunkhwa, Pakistan, *Int. J. Econ. Environ. Geol.*, 72 (2019) 232–243.
- [4] M.S. Achary, K.K. Satpathy, S. Panigrahi, A.K. Mohanty, R.K. Padhi, S. Biswas, R.C. Panigrahy, Concentration of heavy metals in the food chain components of the nearshore coastal waters of Kalpakkam, southeast coast of India, *Food Control*, 72 (2017) 232–243.
- [5] B. de Campos Ventura-Camargo, M.A. Marin-Morales, Azo dyes: characterization and toxicity—a review, *TLIST*, 2 (2013) 85–103.
- [6] R.D. Saini, Synthetic textile dyes: constitution, dyeing process and environmental impacts, *CL, Asian J. Res. Chem. (AJRC)*, 70 (2018) 5–30.
- [7] P.S. Kumar, G.J. Joshiba, Environmental and Health Effects Due to the Usage of Wastewater, In *Life Cycle Assessment of Wastewater Treatment*, CRC Press, United States, 2018, pp. 1–21.
- [8] S. Mishra, R.N. Bharagava, N. More, A. Yadav, S. Zainith, S. Mani, P. Chowdhary, Heavy Metal Contamination: An Alarming Threat to Environment and Human Health, In *Environmental Biotechnology: For Sustainable Future*, Springer, Singapore, 2019, pp. 103–125.
- [9] J. Nawab, S. Khan, S. Ali, H. Sher, Z. Rahman, K. Khan, A. Ahmad, Health risk assessment of heavy metals and bacterial contamination in drinking water sources: a case study of Malakand Agency, Pakistan, *Environ. Monit. Assess.*, 188 (2016) 286.
- [10] H.Y. Hu, Y. Du, Q.Y. Wu, X. Zhao, X. Tang, Z. Chen, Differences in dissolved organic matter between reclaimed water source and drinking water source, *Sci. Total Environ.*, 551 (2016) 133–142.
- [11] N.J. Ashbolt, Microbial contamination of drinking water and human health from community water systems, *Curr. Environ. Health Rep.*, 2 (2015) 95–106.
- [12] M.K. Daud, M. Nafees, S. Ali, M. Rizwan, R. A. Bajwa, M.B. Shakoar, I. Malook, Drinking water quality status and contamination in Pakistan, *BioMed Res. Int.*, 2017 (2017) 7908183 (1–18).
- [13] Food and Agriculture Organization of the United Nations, The State of World Fisheries and Aquaculture 2018—Meeting the Sustainable Development Goals, FAO, United States, 2018.
- [14] S. Sankar, S. Sekar, R. Mohan, S. Rani, J. Sundaraseelan, T.P. Sastry, Preparation and partial characterization of collagen sheet from fish (*Lates calcarifer*) scales, *Int. J. Biol. Macromol.*, 42 (2008) 6–9.
- [15] J. Kozłowska, A. Sionkowska, J. Skopinska-Wisniewska, K. Piechowicz, Northern pike (*Esox lucius*) collagen: extraction, characterization and potential application, *Int. J. Biol. Macromol.*, 81 (2015) 220–227.
- [16] S. Sancilio, M. Gallorini, C. Di Nisio, E. Marsich, R. Di Pietro, H. Schweikl, A. Cataldi, Alginate/hydroxyapatite-based nanocomposite scaffolds for bone tissue engineering improve dental pulp biomineralization and differentiation, *Stem Cells Int.*, (2018).
- [17] S. Sathiskumar, S. Vanaraj, D. Sabarinathan, K. Preethi, Evaluation of antibacterial and antibiofilm activity of synthesized zinc-hydroxyapatite biocomposites from *Labeo rohita* fish scale waste, *Mater. Res. Express*, 5 (2018) 025407.
- [18] L. Berzina-Cimdina, N. Borodajenko, Research of calcium phosphates using Fourier transform infrared spectroscopy, *IR Mater. Sci. Eng. Technol.*, 12 (2012) 251–263.
- [19] S.L. Pandharipande, S.S. Sondawale, Review on synthesis of hydroxyapatite and its bio-composites, *Int. J. Sci. Technol. Res.*, 5 (2016) 3410–3416.
- [20] M. Sutha, K. Sowndarya, M. Chandran, D. Yuvaraj, B. Bharathiraja, R.P. Kumar, Synthesis of Value-Added Biomimetic Material of Hydroxyapatite Using Aqueous Calcareous Fish Wastes, In *Waste to Wealth*, Springer, Singapore, 2018, pp. 59–64.
- [21] A. Pal, K. Hadagalli, P. Bhat, V. Goel, S. Mandal, Hydroxyapatite—a promising sunscreen filter, *J. Aust. Ceram. Soc.*, 56 (2019) 1–7.
- [22] S. Campisi, M.G. Galloni, F. Bossola, A. Gervasini, Comparative performance of copper and iron functionalized hydroxyapatite catalysts in NH₃-SCR, *Catal. Commun.*, 123 (2019) 79–85.
- [23] Y. Li, L.L. Chen, X.X. Lian, J.W. Zhu, Preparation and characterisation of ZnO/HAP bioceramics with excellent antibacterial property, *Mater. Technol.*, 34 (2019) 415–422.
- [24] N. Ma, X. Fan, X. Quan, Y. Zhang, Ag–TiO₂/HAP/Al₂O₃ bioceramic composite membrane: fabrication, characterization and bactericidal activity, *J. Membr. Sci.*, 336 (2009) 109–117.
- [25] Y. Li, H. Zhou, G. Zhu, C. Shao, H. Pan, X. Xu, R. Tang, Highly efficient multifunctional Ag₃PO₄ loaded hydroxyapatite nanowires for water treatment, *J. Hazard. Mater.*, 299 (2015) 379–387.
- [26] L. Dong, Z. Zhu, Y. Qiu, J. Zhao, Removal of lead from aqueous solution by hydroxyapatite/magnetite composite adsorbent, *Chem. Eng. J.*, 165 (2010) 827–834.
- [27] M. Mahdavi-Roshan, M. Ebrahimi, A. Ebrahimi, Copper, magnesium, zinc and calcium status in osteopenic and osteoporotic post-menopausal women, *Clin. Cases Miner. Bone Metab.*, 12 (2015) 18.
- [28] O.H. Ojeda-Niño, C. Blanco, C.E. Daza, High temperature CO₂ capture of hydroxyapatite extracted from tilapia scales, *Univ. Sci.*, 22 (2017) 215–236.
- [29] S. Sathiskumar, S. Vanaraj, D. Sabarinathan, S. Bharath, G. Sivarasan, S. Arulmani, V.K. Ponnusamy, Green synthesis of biocompatible nanostructured hydroxyapatite from *Cirrhinus mrigala* fish scale—a biowaste to biomaterial, *Ceram. Int.*, 45 (2019) 7804–7810.
- [30] N. Mustafa, M.H.I. Ibrahim, R. Asmawi, A.M. Amin, Hydroxyapatite Extracted from Waste Fish Bones and Scales via Calcination Method, In *Applied Mechanics Materials*, Vol. 773, 2015, pp. 287–290.
- [31] A.T. Adesoji, J.P. Onuh, J. Bagu, S.A. Itohan, Prevalence and antibiogram study of *Staphylococcus aureus* isolated from clinical and selected drinking water of Dutsin-Isa, Katsina state, Nigeria, *Afr. Health Sci.*, 19 (2019) 1385–1392.
- [32] N. Ayawei, A.N. Ebelegi, D. Wankasi, Modelling and interpretation of adsorption isotherms, *J. Chem.*, 2017 (2017) 3039817 (1–11).
- [33] S. Zulfikar, U. Rafique, M.J. Akhtar, Removal of pirimicarb from agricultural wastewater using cellulose acetate–modified ionic liquid membrane, *Environ. Sci. Pollut. Res.*, 26 (2019) 15795–15802.
- [34] S.E. Abd Elhafez, H.A. Hamad, A.A. Zaatout, G.F. Malash, Management of agricultural waste for removal of heavy metals from aqueous solution: adsorption behaviors, adsorption mechanisms, environmental protection, and techno-economic analysis, *Environ. Sci. Pollut. Res.*, 24 (2017) 1397–1415.
- [35] H. Shokry, H. Hamad, Effect of superparamagnetic nanoparticles on the physicochemical properties of nano hydroxyapatite for groundwater treatment: adsorption mechanism of Fe(II) and Mn (II), *RSC Adv.*, 6 (2016) 82244–82259.
- [36] H. Gheisari, E. Karamian, M. Abdollahi, A novel hydroxyapatite–hardystonite nanocomposite ceramic, *Ceram. Int.*, 41 (2015) 5967–5975.
- [37] M. Manoj, D. Mangalaraj, N. Ponpandian, C. Viswanathan, Core-shell hydroxyapatite/Mg nanostructures: surfactant free facile synthesis, characterization and their in vitro cell viability studies against leukaemia cancer cells (K562), *RSC Adv.*, 5 (2015) 48705–48711.

- [38] S. Kuśnieruk, J. Wojnarowicz, A. Chodara, T. Chudoba, S. Gierlotka, W. Lojkowski, Influence of hydrothermal synthesis parameters on the properties of hydroxyapatite nanoparticles, *BJNANO*, 7 (2016) 1586–1601.
- [39] M. Chahkandi, Mechanism of Congo red adsorption on new sol-gel-derived hydroxyapatite nanoparticle, *Mater. Chem. Phys.*, 202 (2017) 340–351.
- [40] A. Fihri, C. Len, R.S. Varma, A. Solhy, Hydroxyapatite: a review of syntheses, structure and applications in heterogeneous catalysis, *Coord. Chem. Rev.*, 347 (2017) 48–76.
- [41] M. Markovic, B.O. Fowler, M.S. Tung, Preparation and comprehensive characterization of a calcium hydroxyapatite reference material, *J. Res. Natl. Inst. Stand. Technol.*, 109 (2004) 553.
- [42] T.M. Yurieva, L.M. Plyasova, V.I. Zaikovskii, T.P. Minyukova, A. Bliak, J.C. van den Heuvel, E.D. Batyrev, In situ XRD and HRTEM studies on the evolution of the Cu/ZnO methanol synthesis catalyst during its reduction and re-oxidation, *Phys. Chem. Chem. Phys.*, 6 (2004) 4522–4526.
- [43] Y. Hou, H. Kondoh, T. Ohta, S. Gao, Size-controlled synthesis of nickel nanoparticles, *Appl. Surf. Sci.*, 241 (2005) 218–222.
- [44] M.R. Abukhadra, M.A. Sayed, A.M. Rabie, S. A. Ahmed, Surface decoration of diatomite by Ni/NiO nanoparticles as hybrid composite of enhanced adsorption properties for malachite green dye and hexavalent chromium, *Colloids Surf., A*, 577 (2019) 583–593.
- [45] B. Gayathri, N. Muthukumarasamy, D. Velauthapillai, S.B. Santhosh, Magnesium incorporated hydroxyapatite nanoparticles: preparation, characterization, antibacterial and larvicidal activity, *Arab. J. Chem.*, 11 (2018) 645–654.
- [46] Z. Rahman, V.P. Singh, The relative impact of toxic heavy metals (THMs)(arsenic (As), cadmium (Cd), chromium (Cr) (VI), mercury (Hg), and lead (Pb)) on the total environment: an overview, *Environ. Monit. Assess.*, 191 (2019) 419.
- [47] M.T. Hayat, M. Nauman, N. Nazir, S. Ali, N. Bangash, Environmental Hazards of Cadmium: Past, Present, and Future, In *Cadmium Toxicity and Tolerance in Plants*, Academic Press, 2019, pp. 163–183.
- [48] R.E. Pătescu, L.T. Busuioc, G. Nechifor, C.M. Simonescu, C. Deleanu, Applicability of chitosan/hydroxyapatite composites for adsorptive removal of lead, copper, zinc and nickel from synthetic aqueous solutions, *UPB Sci. Bull. Ser. B*, 79 (2017) 119–134.
- [49] A.S. Sartape, A.M. Mandhare, V.V. Jadhav, P.D. Raut, M.A. Anuse, S.S. Kolekar, Removal of malachite green dye from aqueous solution with adsorption technique using *Limonia acidissima* (wood apple) shell as low-cost adsorbent, *Arab. J. Chem.*, 10 (2017) S3229–S3238.
- [50] U. Shanker, M. Rani, V. Jassal, Degradation of hazardous organic dyes in water by nanomaterials, *Environ. Chem. Lett.*, 5 (2017) 623–642.
- [51] A.M. Al-Sabagh, Y.M. Moustafa, A. Hamdy, H.M. Killa, R.T.M.R.E. Ghanem, Morsi, Preparation and characterization of sulfonated polystyrene/magnetite nanocomposites for organic dye adsorption, *Egypt. J. Pet.*, 27 (2018) 403–413.
- [52] V. Stanić, S. Dimitrijević, J. Antić-Stanković, M. Mitrić, B. Jokić, I.B. Plečaš, S. Raičević, Synthesis, characterization and antimicrobial activity of copper and zinc-doped hydroxyapatite nano powders, *Appl. Surf. Sci.*, 256 (2010) 6083–6089.
- [53] P. Zhang, Adsorption and Desorption Isotherms, KE Group, Thailand, 2016.
- [54] A.A. El-Zahhar, N.S. Awwad, Removal of malachite green dye from aqueous solutions using organically modified hydroxyapatite, *J. Environ. Chem. Eng.*, 4 (2016) 633–638.
- [55] S.D. Khattri, M.K. Singh, Removal of malachite green from dye wastewater using neem sawdust by adsorption, *J. Hazard. Mater.* 167 (2009) 1089–1094.
- [56] K. Parveen, U. Rafique, S.Z. Safi, M.A. Ashraf, A novel method for synthesis of functionalized hybrids and their application for wastewater treatment, *Desal. Water Treat.*, 57 (2016) 161–170.
- [57] K. Sangeetha, G. Vidhya, G. Vasugi, E.K. Girija, Lead and cadmium removal from single and binary metal ion solution by novel hydroxyapatite/alginate/gelatin nanocomposites, *J. Environ. Chem. Eng.*, 6 (2018) 1118–1126.
- [58] D. Robati, Pseudo-second-order kinetic equations for modeling adsorption systems for removal of lead ions using multi-walled carbon nanotube, *JNSC*, 3 (2013) 55.

Supporting information

Table S1

Fourier transform infrared spectroscopy data of HAp (CC)

Serial no.	Sample name	Obtained peaks (cm ⁻¹)	Indicated functional groups	References
01	HAp powder (CC)	3,416.05	O–H stretch (broad, s)	[36]
		1,662.69	H ₂ O	[17]
		1,465.95	CO ₃ ²⁻	[17]
		1,043.62	O–P–O PO ₄ ³⁻	[37]
		866.07	CO ₃ ²⁻	[17]
		603.74	O–H bend	[36]
		565.16	O–P–O PO ₄ ³⁻	[37]



Fig. S1. Catalase positive test.

Table S2
Particle size data conversion

Sample	X-ray diffraction data			
	2 θ	FWHM	d-spacing	Crystallite size
CuHAP 3% CC	25.340	0.253	0.351	33.856
	36.058	0.425	0.248	20.145
	37.202	0.396	0.241	21.605
	38.517	0.305	0.233	28.049
	40.643	0.413	0.221	20.729
	43.240	0.416	0.208	20.587
Average crystallite size = 24.162 nm				
NiHAp 3% CC	25.262	0.239	0.352	0.352
	32.516	0.245	0.275	0.275
	35.931	0.525	0.249	0.249
	37.138	0.406	0.241	0.241
	38.470	0.177	0.233	0.233
	40.566	0.391	0.222	0.222
	43.175	0.451	0.209	0.209
	53.032	0.554	0.172	0.172
62.853	0.753	0.147	0.147	
Average crystallite size = 25.596 nm				
HAp (CC)	25.866	0.610	0.344	13.930
	31.886	0.920	0.280	9.374
	41.986	0.231	0.214	38.361
	49.532	0.647	0.183	14.108
	63.960	0.693	0.145	14.094
Average crystallite size = 17.973 nm				

FWHM: full width half maximum; XRD: X-ray diffraction.

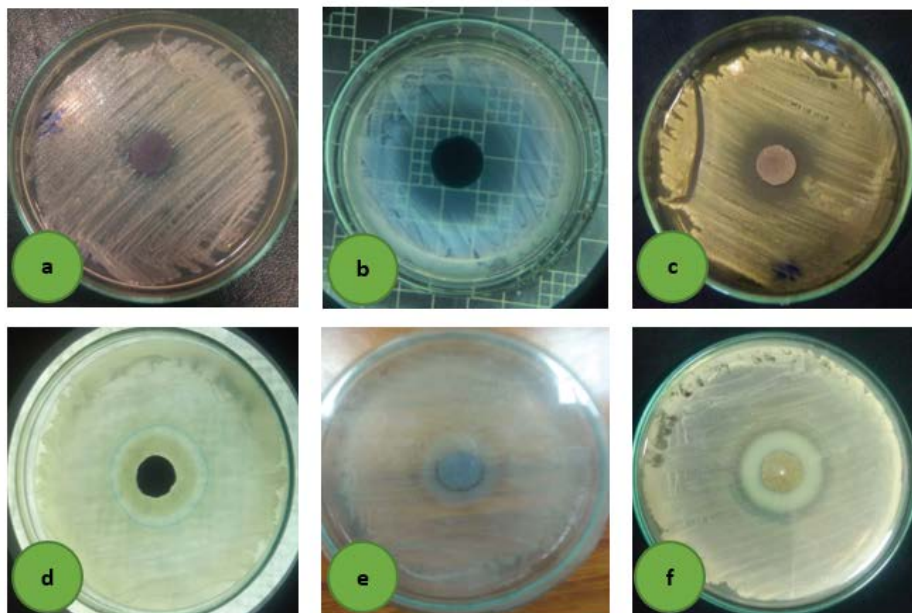


Fig. S2. Inhibition zones; (a–c): Cu-HAp 1:1 (1 wt.% metal), Cu-HAp 3:1 (3 wt.% metal), Cu-HAp 1:3 (1 wt.% metal), respectively, (d–f): Ni-HAp 1:1 (1 wt.% metal), Ni-HAp 3:1 (3 wt.% metal), Ni-HAp 1:3 (1 wt.% metal), respectively.

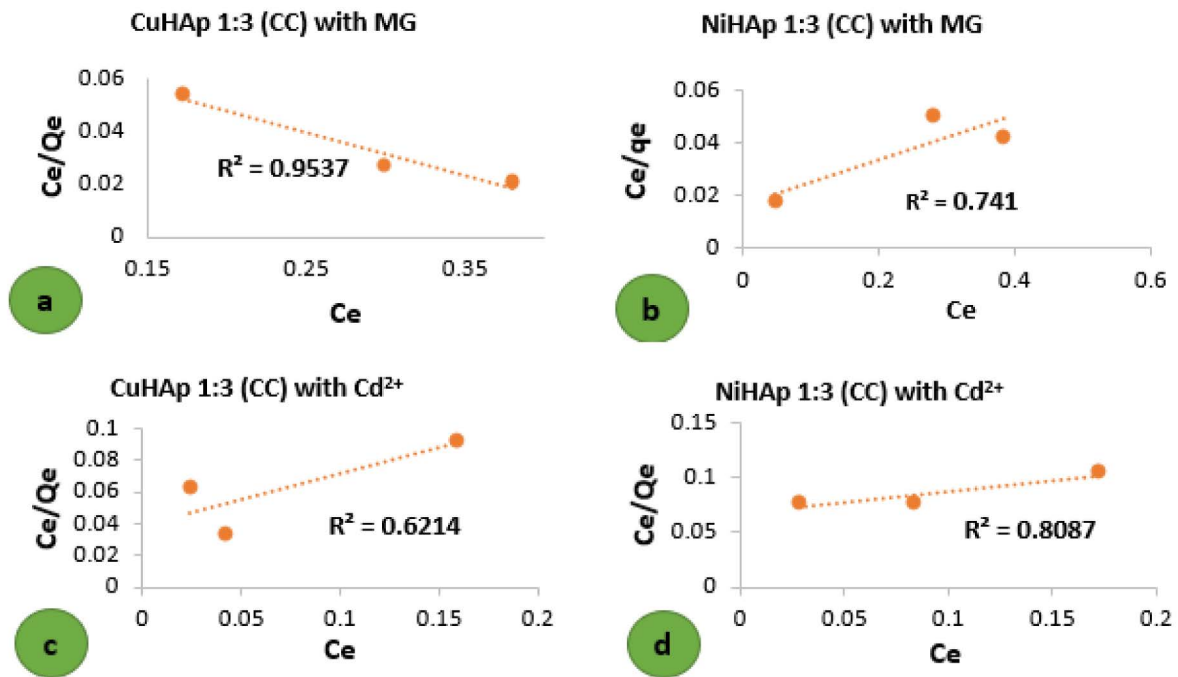


Fig. S3. Langmuir isotherms; (a and b): CuHAp 1:3 (CC) and NiHAp 1:3 (CC) with MG; (c and d): CuHAp 1:3 (CC) and NiHAp 1:3 (CC) with Cd^{2+} , respectively.

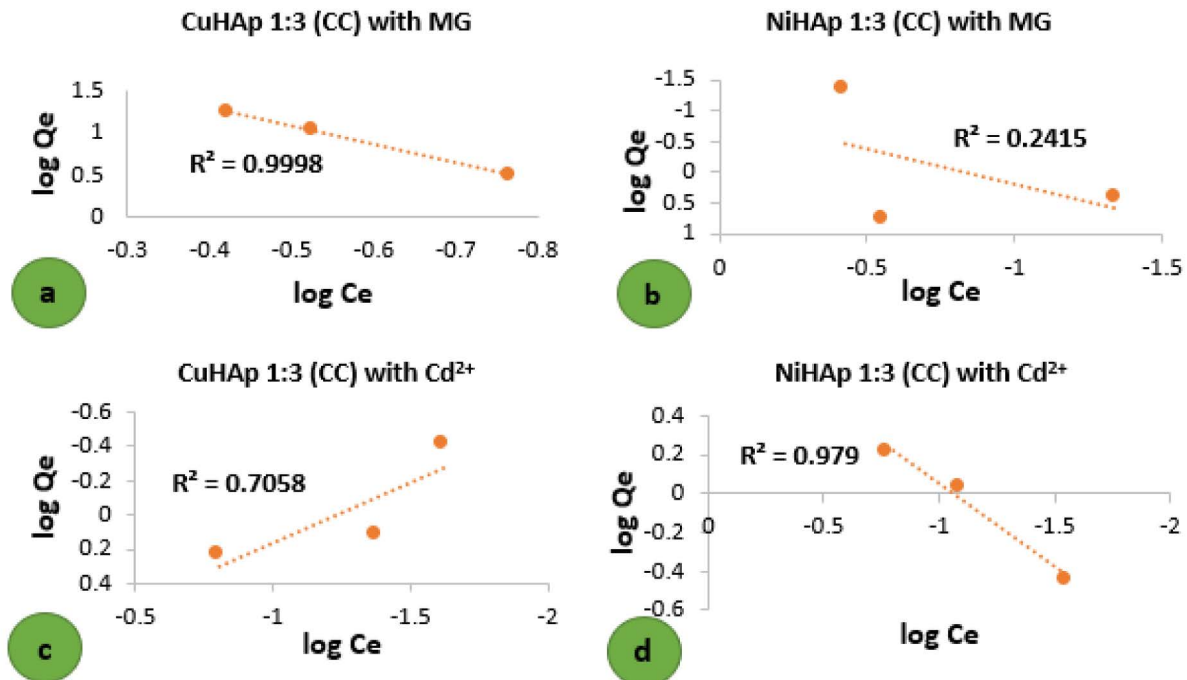


Fig. S4. Freundlich isotherms; (a and b): CuHAp 1:3 (CC) and NiHAp 1:3 (CC) with MG; (c and d): CuHAp 1:3 (CC) and NiHAp 1:3 (CC) with Cd^{2+} , respectively.

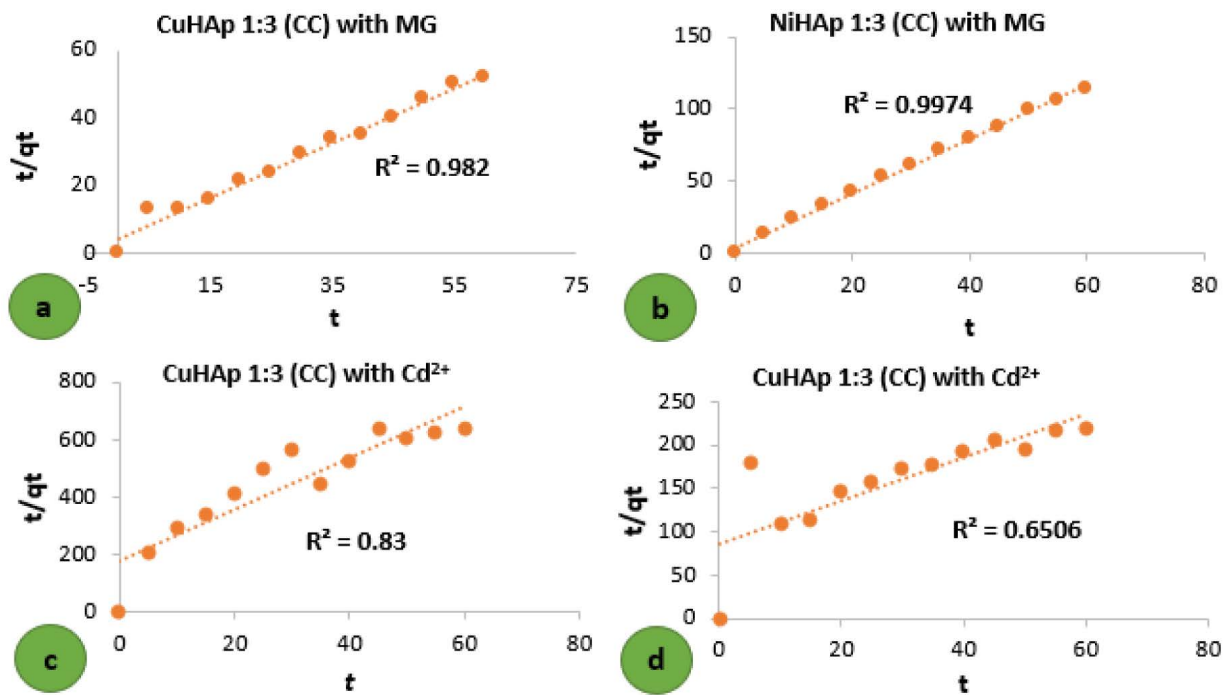


Fig. S5. Pseudo-second order; (a and b): CuHAp 1:3 (CC) and NiHAp 1:3 (CC) with MG; (c and d): CuHAp 1:3 (CC) and NiHAp 1:3 (CC) with Cd^{2+} , respectively.

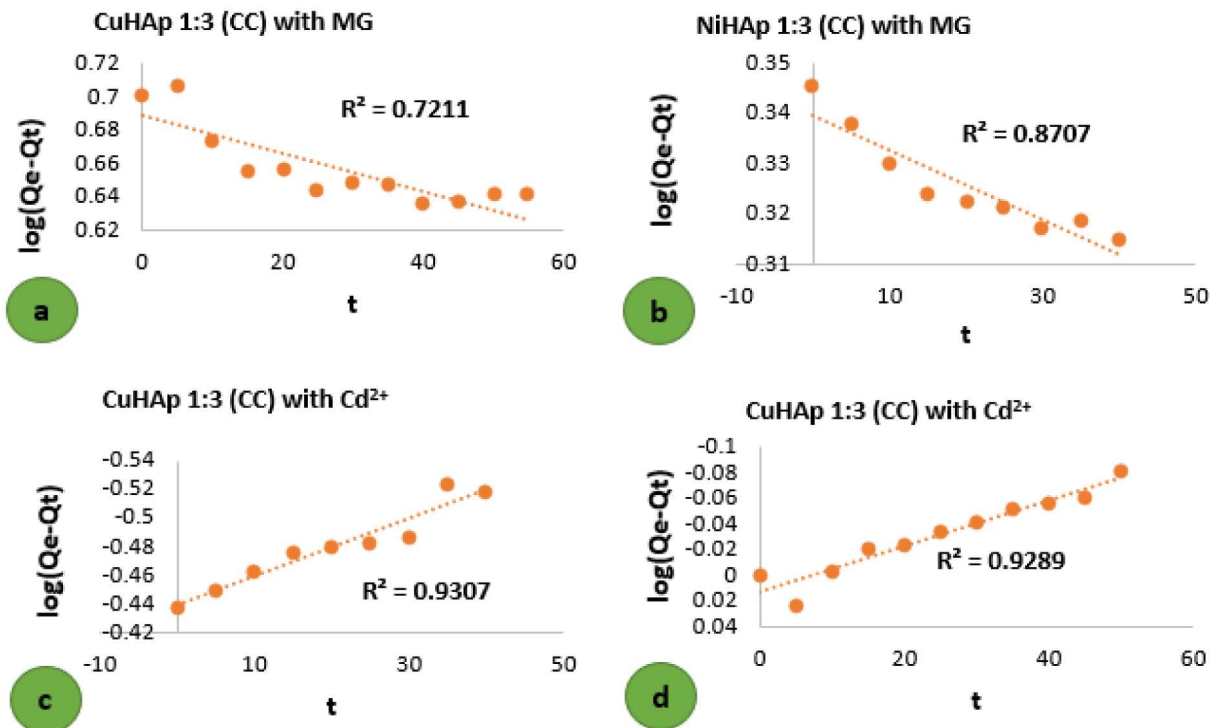


Fig. S6. First order; (a and b): CuHAp 1:3 (CC) and NiHAp 1:3 (CC) with MG; (c and d): CuHAp 1:3 (CC) and NiHAp 1:3 (CC) with Cd^{2+} , respectively.

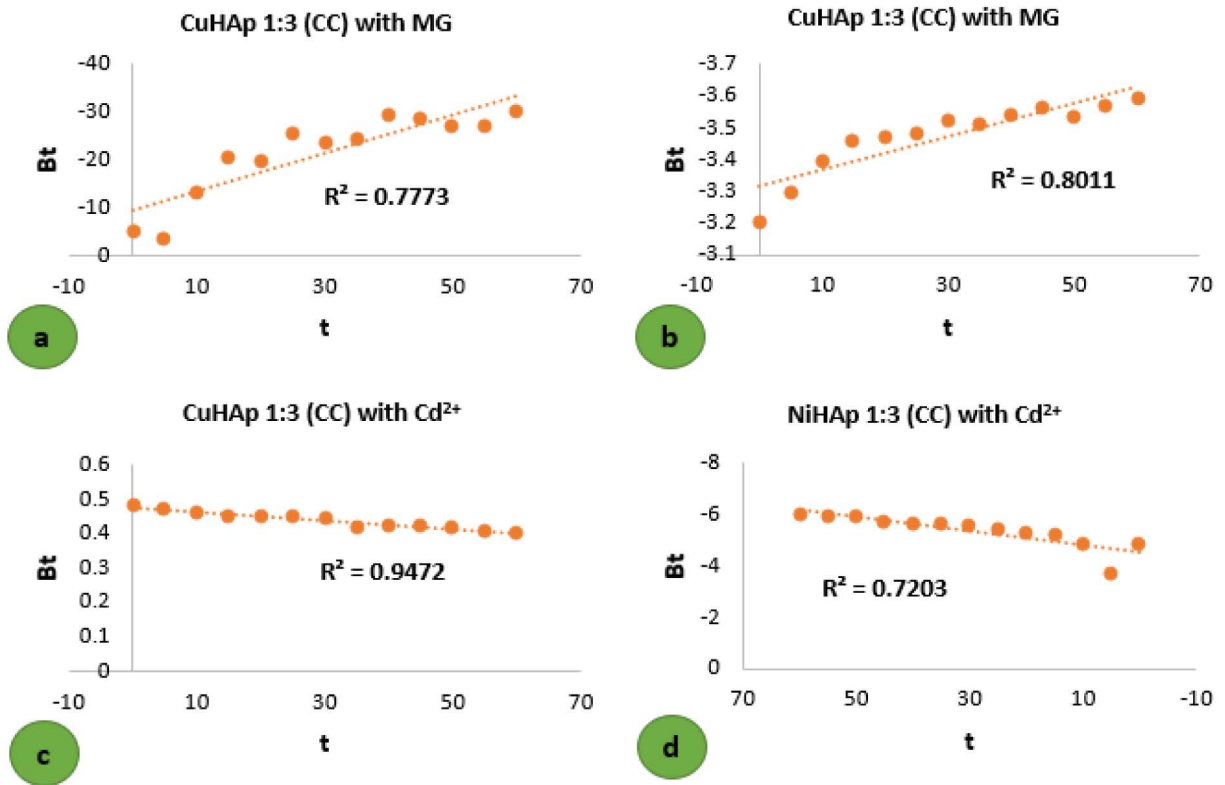


Fig. S7. Boyd plot; (a and b): CuHAp 1:3 (CC) and NiHAp 1:3 (CC) with MG; (c and d): CuHAp 1:3 (CC) and NiHAp 1:3 (CC) with Cd^{2+} , respectively.